

Noise Tolerance of Improved Max-min Scanning Method for Phase Determination

Xu Ding

Research Assistant

Mechanical Engineering Dept., Michigan State University, East Lansing, MI, 48824, USA

Gary L. Cloud, P.E.

Professor

Mechanical Engineering Dept., Michigan State University, East Lansing, MI, 48824, USA

Basavaraju B. Raju

Senior Research Engineer

US Army Tank Automotive Command, Warren, MI, 48397, USA

ABSTRACT

This paper presents and demonstrates the enhancement of noise tolerance exhibited by the improved Max-Min scanning method (IMMS) for phase determination. Numerical simulations and various tests indicate that the IMMS has a good tolerance to certain ranges of noise. One of the IMMS applications, an online method to calibrate the phase shifter, is presented as well. This improved algorithm provides an easy and convenient way to inspect the linearity and the non-uniformity of the phase shifter. It is suitable for use in assessing the reliability of the phase shifting setup in real time.

INTRODUCTION

The phase shifting technique is a key step in optical measurement. An improved Max-Min scanning method has been described by Ding and Cloud [1, 2]. The principle of it is briefly reviewed in the next section. There is always a serious concern about the environmental tolerance of all kinds of phase determination techniques, because the noise tolerance establishes the limitations on the range of application of the phase shifting techniques. The majority of current techniques require a vibration-isolated table. This paper shows that the application of low-pass filtering and curve fitting techniques to the recorded signals in the time domain improves the noise tolerance of the developed IMMS method. Numerical simulations and tests are presented.

One useful application of the IMMS approach is presented in this paper also: calibration of the phase shifter. Generally, a phase shifter, which is usually a mirror mounted on a piezoelectric transducer (PZT), is used to vary one beam path length artificially so as to vary the phase difference between the interfering beams by some supposedly known amount, and then some intensity image signals are captured to calculate the expected phase information [2,3,4,5,6,7]. Although some of these techniques were claimed to be insensitive to phase shifting errors, an efficient real-time calibration of the phase shifter is still desired to understand the effectiveness of the phase shifter and to make phase shifting techniques more accurate. The working status of the phase shifter, such as the demanded driving voltage, non-linearity, stability of the PZT, and the tilt of the mirror, will more or less affect the accuracy of the measurement results. In the past decades, several calibration methods have been developed. They have been categorized into two classes: fringe tracking and the Carré method as described by Hedser Van Brug [8,9]. The fringe locking method is mainly suited with an accurate 2π phase step. The Carré method uses several phase-stepped images to calculate the phase shifting angle by assuming that the phase shifter is linear and uniform, which is likely not true. Neither of these two methods is able to provide the linearity, the tilt, and the non-uniformity of the phase shifter.

In this paper, a new real-time calibration method is proposed to calibrate the phase shifting apparatus, as well as to inspect the non-linearity, tilt and non-uniformity of the phase shifter's movement.

IMMS METHOD

The principle of the IMMS method is briefly given as follows [1]. The intensity equation of an interferogram is written as

$$I = I_1 + I_2 + 2\sqrt{I_1 I_2} \cos(\phi) \quad (1)$$

Report Documentation Page

Form Approved
OMB No. 0704-0188

Public reporting burden for the collection of information is estimated to average 1 hour per response, including the time for reviewing instructions, searching existing data sources, gathering and maintaining the data needed, and completing and reviewing the collection of information. Send comments regarding this burden estimate or any other aspect of this collection of information, including suggestions for reducing this burden, to Washington Headquarters Services, Directorate for Information Operations and Reports, 1215 Jefferson Davis Highway, Suite 1204, Arlington VA 22202-4302. Respondents should be aware that notwithstanding any other provision of law, no person shall be subject to a penalty for failing to comply with a collection of information if it does not display a currently valid OMB control number.

| | | | | | |
|---|------------------------------------|--|----------------------------|---|---------------------------------|
| 1. REPORT DATE 04 JUN 2004 | | 2. REPORT TYPE Journal Article | | 3. DATES COVERED 04-03-2004 to 08-04-2004 | |
| 4. TITLE AND SUBTITLE Noise Tolerance of Improved Max-min Scanning Method for Phase Determination | | | | 5a. CONTRACT NUMBER | |
| | | | | 5b. GRANT NUMBER | |
| | | | | 5c. PROGRAM ELEMENT NUMBER | |
| 6. AUTHOR(S) Xu Ding; Gary Cloud; Basavaraju Raju | | | | 5d. PROJECT NUMBER | |
| | | | | 5e. TASK NUMBER | |
| | | | | 5f. WORK UNIT NUMBER | |
| 7. PERFORMING ORGANIZATION NAME(S) AND ADDRESS(ES) Mechanical Engineering Dept., Michigan State University, 428 S. Shaw Lane, Rm. 2555, East Lansing, Mi, 48824 | | | | 8. PERFORMING ORGANIZATION REPORT NUMBER ; #14180 | |
| | | | | 10. SPONSOR/MONITOR'S ACRONYM(S) TARDEC | |
| 9. SPONSORING/MONITORING AGENCY NAME(S) AND ADDRESS(ES) U.S. Army TARDEC, 6501 East Eleven Mile Rd, Warren, Mi, 48397-5000 | | | | 11. SPONSOR/MONITOR'S REPORT NUMBER(S) #14180 | |
| | | | | | |
| 12. DISTRIBUTION/AVAILABILITY STATEMENT Approved for public release; distribution unlimited | | | | | |
| 13. SUPPLEMENTARY NOTES | | | | | |
| 14. ABSTRACT This paper presents and demonstrates the enhancement of noise tolerance exhibited by the improved Max-Min scanning method (IMMS) for phase determination. Numerical simulations and various tests indicate that the IMMS has a good tolerance to certain ranges of noise. One of the IMMS applications, an online method to calibrate the phase shifter, is presented as well. This improved algorithm provides an easy and convenient way to inspect the linearity and the non-uniformity of the phase shifter. It is suitable for use in assessing the reliability of the phase shifting setup in real time. | | | | | |
| 15. SUBJECT TERMS | | | | | |
| 16. SECURITY CLASSIFICATION OF: | | | 17. LIMITATION OF ABSTRACT | 18. NUMBER OF PAGES | 19a. NAME OF RESPONSIBLE PERSON |
| a. REPORT unclassified | b. ABSTRACT unclassified | c. THIS PAGE unclassified | | | |

where I is the intensity at one pixel, I_1 and I_2 are the intensities of the two interfering beams respectively, and ϕ is the phase difference between these two interfering beams at that pixel [3].
 From equation (1), the phase angle can be derived as:

$$\phi = \text{ArcCos} \left(\frac{I - \frac{I_{Max} + I_{Min}}{2}}{\frac{I_{Max} - I_{Min}}{2}} \right) \quad (2)$$

In this equation, I represents the intensity at one pixel. I_{Max} and I_{Min} are respectively the maximum and minimum values of the pixel intensity at the same pixel position as I .

By changing the driving voltage to the PZT phase shifter, the phase difference ϕ between the two interfering beams can be artificially varied, and at the same time, the digital pictures of the light intensity of the interfering speckle image for each mirror location are recorded. After recording, plot the light intensity values versus driving voltage at each pixel position. Low-pass filtering and least-square curve fitting methods are used to remove noise and fit the intensity curve. The smooth intensity variation curve is obtained. On this wave curve, the gradient is computed at each point, and then the peak values and valley values are determined, these being the maximum and minimum intensity values respectively. The phase value ϕ at each point can be determined through equation (2).

On the fitting curve, the derivative value at the point where driving voltage equals zero is calculated to determine the quadrant of ϕ . If the derivative is positive, then reverse the sign of phase ϕ obtained from equation (2) to put the phase angle in quadrant 3 or quadrant 4. Otherwise, put the phase ϕ in quadrant 1 or quadrant 2. The above processing is performed at each pixel over the entire image. The phase map is determined.

THE NOISE TOLERANCE PROPERTY OF THE IMMS METHOD

Since some numerical filters, for instance a low pass filter, can be employed to process the recorded intensity signals in the time domain, a good noise tolerance is expected for this IMMS method. At ten points chosen randomly over the entire image, good intensity variation curves are recorded by driving the PZT mirror in an in-plane DSPI setup where the setup and specimen are all on a vibration insulated table. Numerical simulations and some real noise signals are used to test the noise tolerance property of this IMMS method at these ten points.

1. Numerical simulation

A numerical Gaussian white noise generator whose standard deviation can be controlled is used to generate some white noise signals. These noise signals are added to the recorded intensity signals. The IMMS method is employed to both the originally recorded intensity signals and the noise-added intensity signals to determine phase values. Results are compared as follows. Figure 1 is a recorded good intensity variation curve. Figure 2 is an example of Gaussian white noise whose standard deviation is 2.0. The RMS signal to noise ratio is 6.3.

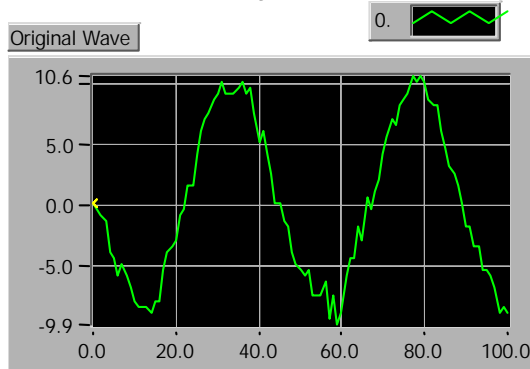


Figure 1. A recorded good intensity changing curve

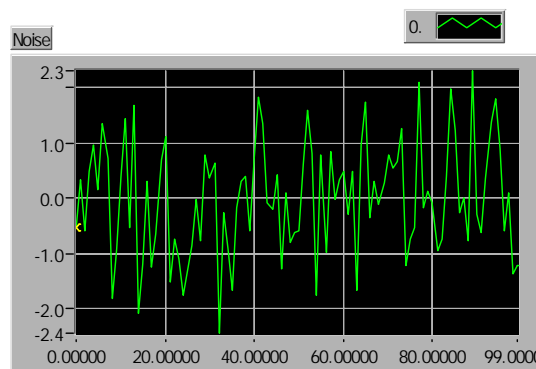


Figure 2. Gaussian white noise signals.

Figure 3 presents the fitted curve of the originally recorded intensity wave. Figure 4 shows the resulting curve from IMMS for the noise-added (Figure 2) intensity signals. The results match well.

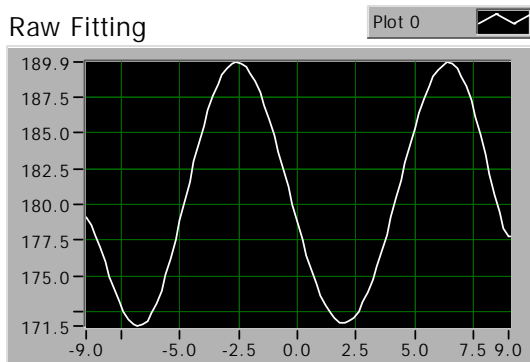


Figure 3. The fitting curve of the original recorded signals.

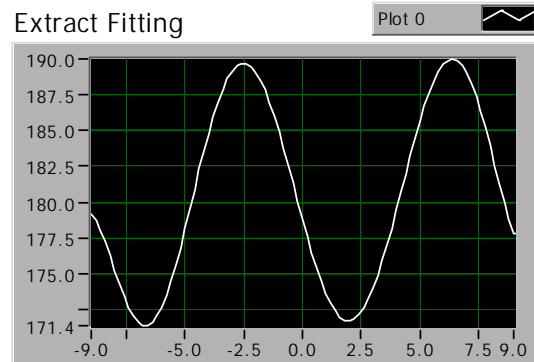


Figure 4. The fitting curve of noise added intensity signals.

The deviation of the noise signals was increased gradually. Figure 5 shows the fitting result for the same recorded intensity signals as in Figure 1 after a noise signal whose deviation is 6.5 was added. Figure 5 shows that the IMMS method cannot efficiently process such a noisy signal. Testing through a range of deviation of the white noise signals shows that the IMMS method can efficiently remove noise having only small deviation.

The same noise having a 6.5 deviation was then filtered by a high pass filter, which means only high frequency noise is left to be added to the original signal. Figure 6 shows that a good result is obtained. This indicates that high frequency noise even with large amplitude can be removed by the IMMS efficiently. Repetition of the simulation tests showed that the IMMS method has very good immunity to both high frequency noise and small amplitude low frequency noise. Large amplitude low frequency noise can damage the efficiency of the noise immunity of the IMMS method.

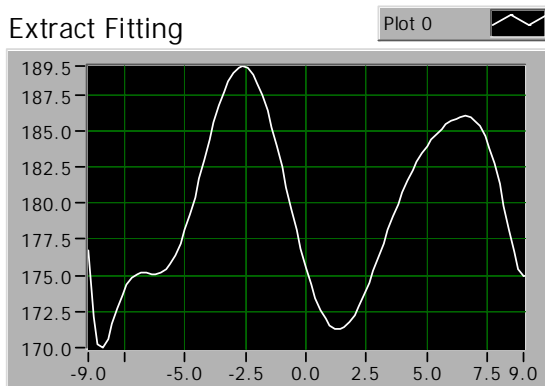


Figure 5. The fitting curve of an intensity wave with a 6.5 deviation noise added.

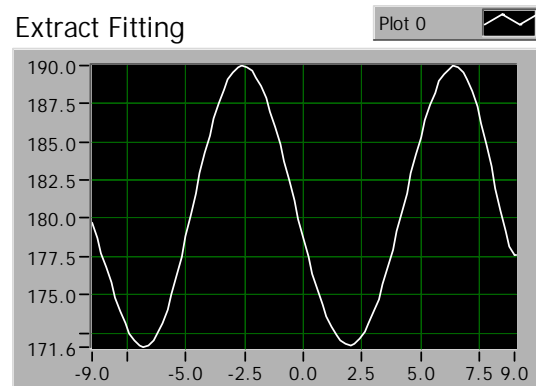


Figure 6. The fitting curve of the intensity wave with a 6.5 deviation high frequency noise added.

2. The effect of real noise signals

At various points on the specimen, the intensity changes induced by environmental noise (such as air turbulence and vibration) were obtained under three different situations by the DSPI setup. The IMMS method was employed to process these noise-added signals.

A. The specimen is placed on a vibration-insulated table:

A noise signal example is shown in Figure 7. This noise is added to a good intensity variation curve (Figure 8). Figure 9 gives the fitting result of the IMMS method. The phase value obtained from the IMMS is -3.14 , which exactly matches the phase

obtained from the original signals. In this example, the RMS signal-to-noise ratio is 7.22 Rad. On this table, the vibration is minute. So, the RMS-SNR is bigger than for other cases. The IMMS works very well in this situation, as expected.

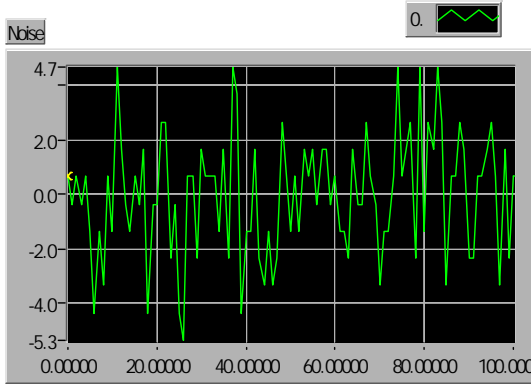


Figure 7. Noise signals under A condition.

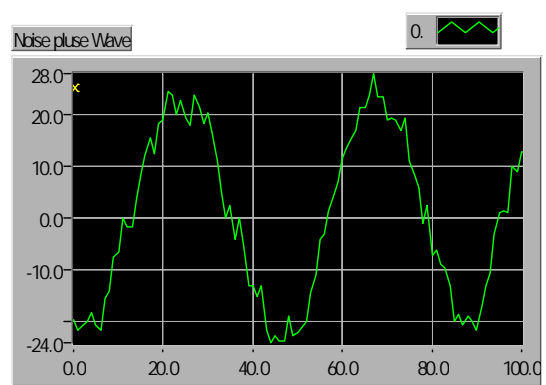


Figure 8. Intensity change curve with noise added.

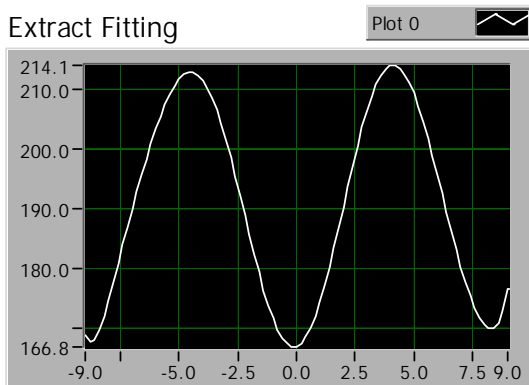


Figure 9. The fitting curve obtained by IMMS.

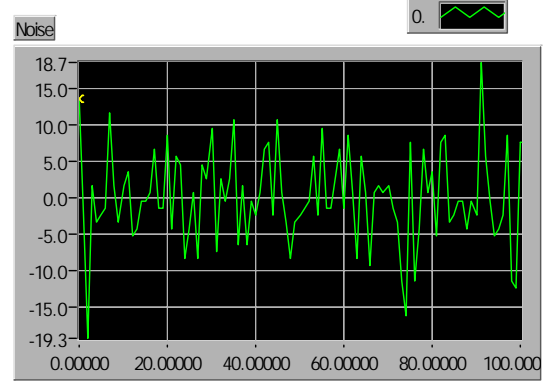


Figure 10. Noise signal.

B. The specimen is put on the same table without air support vibration isolation:

Figure 10 is an example of noise signals under this situation. The original intensity curves is distorted more than the previous one by the noise (Figure 11). Figure 12 shows the IMMS result. The RMS-SNR is 1.81. The phase result still matches exactly at -2.29 Rad. In this situation, the specimen vibration is much more serious. Therefore, the RMS-SNR is smaller than the previous case, around 1.8. However, the IMMS still works well.

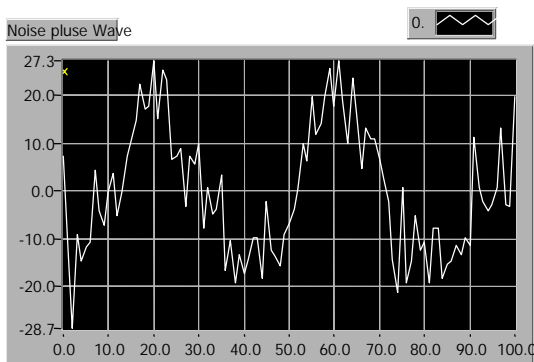


Figure 11. Intensity curve with noise added.

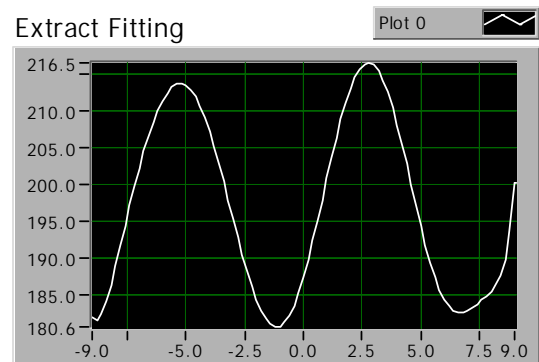


Figure 12. The IMMS result.

C. Noise recorded with the specimen placed on a cart.

In this case, the specimen was placed on an ordinary laboratory cart that is very susceptible to environment noise, especially the vibrations. Noise signals were recorded at various points and much bigger variances were observed for these noise signals, as expected (see Figure 13, which has a 30.62 variance).

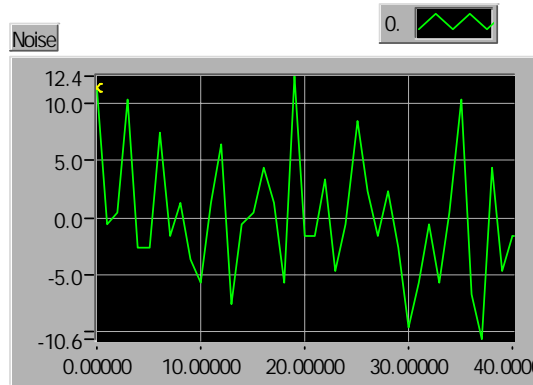


Figure 13. Noise sample obtained under case C.

In this situation, an alternative calibration was used to measure in-plane displacement of a plate. The recorded noise signals were added to each pixel over the whole image during displacement measurement by the IMMS algorithm. The same displacement calibration set up as in reference [10] was used to introduce known in-plane displacement. Table 1 gives some examples of these test results. It indicates that the IMMS worked well even under these high noise conditions.

Table 1. Some examples of displacement measurements

| Variance of noise | Induced known displacement (μm) | Measured displacement by the IMMS (μm) | Error (%) |
|-------------------|--|---|-----------|
| 30.62 | 1.864 | 1.85 | -0.75107 |
| 37.75 | 1.682 | 1.75 | 4.042806 |
| 30.23 | 2.704 | 2.82 | 4.289941 |

All the above simulations were repeated tens of times at different dates and times. The IMMS method proved to have a good ability to reduce certain specific noise effects. Especially, the IMMS method reliably removes high frequency noise and small amplitude low frequency noise. The noise immunity ability of the newly developed IMMS method makes the DSPI technique more practical.

4. Application of IMMS to PZT calibration

By applying the phase determination computation presented in section 2 at all points along the entire intensity curve, the plot of phase values versus driving voltages is obtained with 2π ambiguity as shown in Figure 14. The phase curve is obtained by performing phase unwrapping with respect to the zero driving voltage point. The phase steps induced by the driving voltages are determined (Figure 15). From Figure 15, the driving voltage required by the PZT to get an expected phase step at this point can be obtained by interpolation of the data. As well, the non-linearity of the phase shifting at this point is displayed on the curve. To calibrate a specific phase step, i.e. $\pi/2$ phase step, the above calibration can be performed at a number of pixel points over the entire image. An average driving voltage to get that phase step can be obtained.

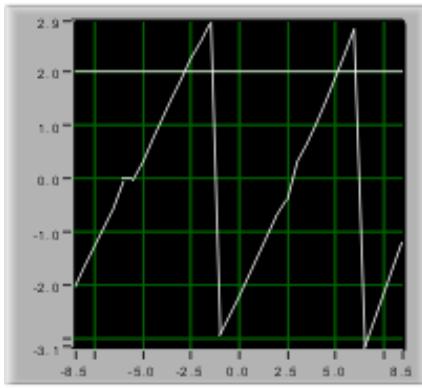


Figure 14. Phase Step with 2π ambiguity.

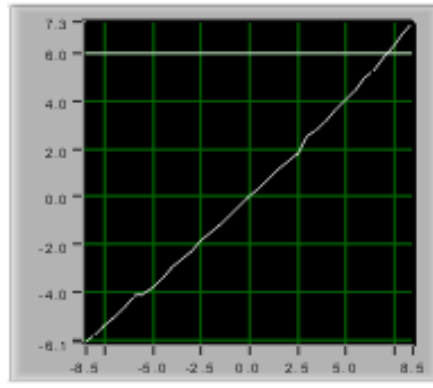


Figure 15. Phase Step VS Driving Voltage.

Tilt and non-uniformity of the phase shifter movement are two other important concerns that significantly affect the accuracy of phase shifting. In this study, at a given driving voltage to the PZT, phase shifting data at points along two perpendicular edges of the image were computed and plotted. The calculation procedure described above was repeated at each point on these two edges to get the phase shifting curves. Figure 16 shows the tilt and non-uniformity of phase shift along the x-axis edge, and Figure 17 is for the y-axis edge. The phase step values corresponding to the calibrated $\pi/2$ driving voltage were combined into a 3-D graph, from which the tilt and non-uniformity of the phase shifter can be assessed visually and directly. Figure 18 is an example of such a 3-D graph.

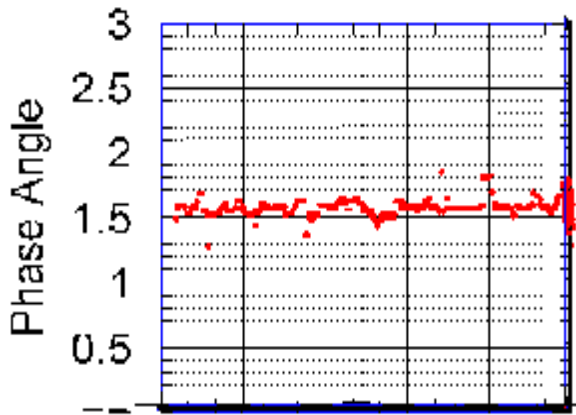


Figure 16. Tilt and uniformity in x direction.

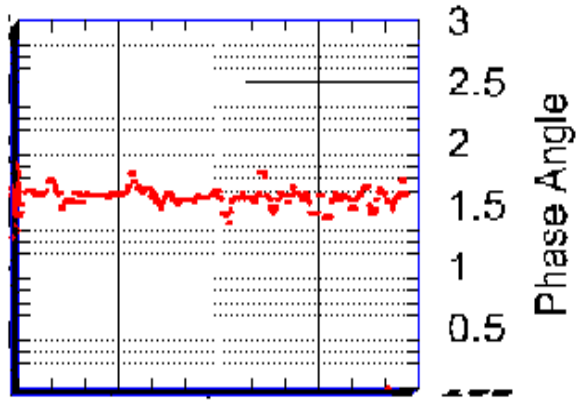


Figure 17. Tilt and uniformity in y direction.

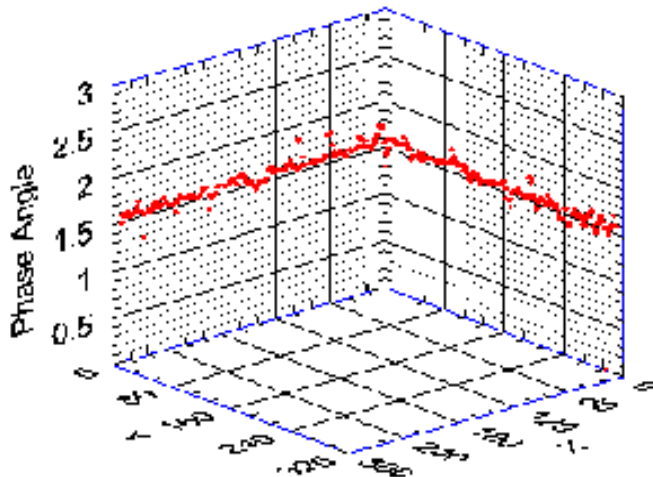


Figure 18. A 3-D plot of the obtained phase shifting results.

The method described above has been used in our lab to calibrate and inspect the phase shifter used in a DSPI setup. Figure 19 represents a recorded intensity wave. After filtering and curve fitting, a smooth waveform was obtained as shown in Figure 20.

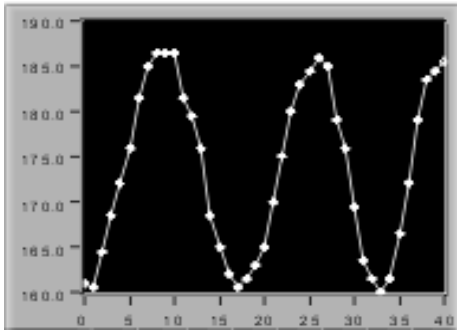


Figure 19. Recorded intensity waveform

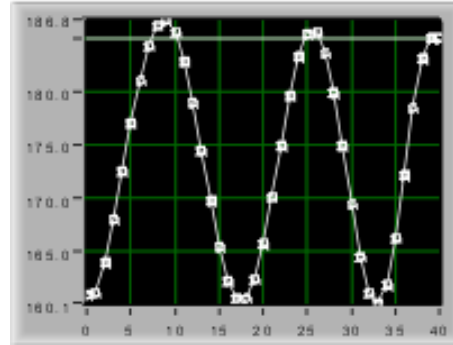


Figure 20. Fitting curve obtained by IMMS

The calibration result is as shown in Figure 15. For this specific experimental setup, the driving voltage to get a $\pi/2$ phase step is 2.09V. Figure 15 shows that the linearity of this phase shifter is good as well. Figures 16, 17 and 18 indicate that the tilt and non-uniformity of this PZT phase shifter are very small.

From the results of hundreds of tests, the average driving voltage to get a $\pi/2$ phase step is determined at 2.13V for this apparatus. The standard deviation is 0.104, which implies very good stability for this setup.

5. Conclusions and Comments

In this paper, the noise tolerance of IMMS method is discussed. It is shown that the IMMS method has a good tolerance to certain noise signals, including high-frequency noise and small-amplitude low-frequency noise. Thus, the IMMS technique facilitates application of interferometric techniques, including DSPI/ESPI, in factory-type environments.

A phase shifting calibration algorithm has been derived from the IMMS method also, and its applications to a PZT phase shifter were successfully demonstrated in some experiments. This algorithm shows several practical advantages. First, it eliminates the drawbacks caused by the common assumptions of linearity and uniformity of the phase shifter, thus efficiently minimizing the movement error of the PZT. Second, it can be used to inspect the working reliability of the phase shifter by showing simultaneously the non-linearity, non-uniformity, and tilt of the phase shifter.

Overall, this new method is a convenient and ideal way to calibrate the phase shifter, as well as to inspect the quality of the phase shifter and the reliability of the experimental setup. Whenever the experimental setup is adjusted, such as by changing the illumination angle or the path length of beam, this algorithm can implement calibration and inspection online.

Acknowledgement

This research was supported by US Army Tank-Automotive Research, Development, and Engineering Center (TARDEC). The authors are grateful to Dr. Douglas Templeton, Team Leader-Emerging Technologies.

References:

1. Ding, X., "Improved signal processing for Max-Min scanning method for phase determination," Student Paper, 2002 SEM Conference on Experimental and Applied mechanics, Milwaukee, WI, 2002.
2. Ding, X., Cloud, G. L., Raju, B. B., "Improved signal processing algorithm for the max-min scanning method for phase determination," *Optical Engineering*, Vol. 43, No. 1, pp. 63-68, 2004.
3. Koliopoulos, C. L., "Phase shifting techniques applied to unique applications," *Proc. SPIE*, Vol. 2861, pp. 86-93, 1996.
4. Cloud, G. L., *Optical Methods of Engineering Analysis*, Cambridge University Press, New York, 1995.
5. Creath, Katherine, "Phase-shifting speckle interferometry," *App. Opt.*, Vol. 24, No. 18, pp. 3053-3058, 1985.
6. Vrooman, H. A. and Maas, A. M., "Image processing algorithms for the analysis of phase shifted speckle interference patterns," *App. Opt.*, Vol. 30, No. 13, pp. 1636-1641, 1991.
7. Sesselmann, M., Goncalves, A. A. Jr., "Single phase step algorithm for phase difference measurement using ESPI," *Proc. SPIE*, Vol. 3478, pp. 153-159, Jul. 1998.
8. Zhang, H., Lalor, M. J. and Burton, D. R., "A new error compensating seven sample phase shifting algorithm and application in 3-D fringe projection profilometry," *Proc. SPIE*, Vol. 3478, pp. 121-132, Jul. 1998.
9. Brug, H. V., "Phase-step calibration for phase-stepped interferometry," *App. Opt.*, Vol. 38, No. 16, pp. 3549-3555, 1999.

10. Cheng, Y. Y. and Wyant, J. C., "Phase shifter calibration in phase-shifting interferometry," *App. Opt.*, Vol. 24, No. 18, pp. 3049-3052, 1985.
11. Cloud, G. L., "Practical speckle interferometry for measuring in-plane deformations," *App. Opt.*, Vol. 14, No. 4, pp. 878-884, 1979.